

Real Time Methods for Wideband Data Processing Based on Surface Acoustic Waves

N. V. Masalsky

*Research Institute of System Researches, Russian Academy of Sciences,
Nakhimovskii pr. 36, korp. 1, Moscow, 117218
Russia*

1. Introduction

The newly developed methods enjoy the advantages of an optical channel for data transfer (parallel data processing in real time, high operating speed, and noise immunity) and the advantages typical of integrated optics (compactness, low power consumption, high sensitivity in information signal processing, stability against external action, and the possibility of using the batch-fabrication technique). The aforesaid advantages account for the wide use of waveguide acoustooptic (AO) units (WAOU) in computing, fiber-optic, telecommunication, and other photonic systems [1-3]. Conventional WAOUs are constructed from 3D elements. However, size, power consumption, and sensitivity to environmental conditions (vibrations, temperature variations, etc.) set limits on the applications of these devices. The WAOU (typical functional scheme is shown on fig. 1) is based on the waveguide AO Bragg diffraction of the modulated light beam on a modulated surface acoustic wave (SAW) and the registration of this diffraction image. One of the main WAOU parameters is product $T_A \Delta f$, where $T_A = W_{opt}/V$ is the maximum delay time, which is known to be equivalent to the propagation time of the SAW leading edge through the optical beams, where W_{opt} is the optical beam width, V - the SAW velocity, and Δf is the working frequency band.

The x axis is directed along the propagation of the optical beam, the y axis is orthogonal to the waveguide plane and directed to its depth, and the z coordinate is perpendicular to the direction of propagation of the optical beam.

SAW operates as an optical driving transparency [4,5]. It executes following important operations:

- changing of deflection angle by means of change of SAW frequency (frequency of applied RF-signal) - this property is used for optical deflectors, scanners, switches;
- changing of intensity of diffracted beam by means of change of power of applied RF-signal - this property is used for amplitude modulation;
- changing of frequency of diffracted beam depended on changing of SAW frequency - frequency modulation.

SAW is generated with an electro-acoustical transducer [6]. The transducer type is usual inter digital transducer (IDT).

Source: Acoustic Waves, Book edited by: Don W. Dissanayake,
ISBN 978-953-307-111-4, pp. 466, September 2010, Sciyo, Croatia, downloaded from SCIYO.COM

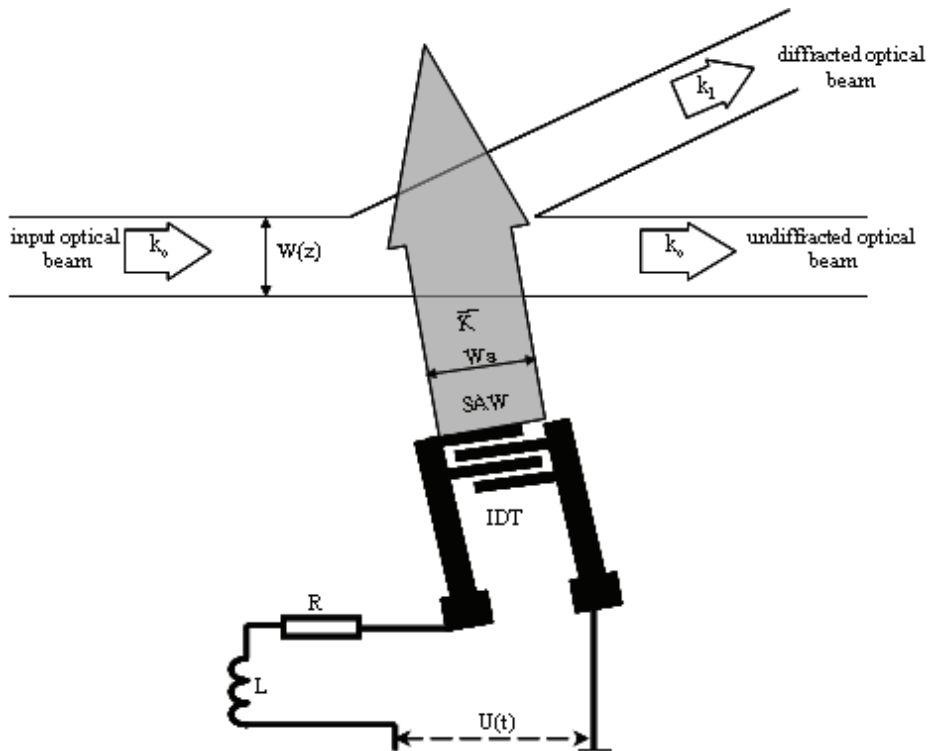


Fig. 1. Functional scheme WAOU, where k_0 , k_1 – optical wave vectors, K – SAW wave vector, $W(z)$ – optical aperture function, W_a – SAW aperture. Solid lines show optical beams. The source of optical radiation, lens system and registration unit are not shown.

The optical wave passes three areas. The optical wave aperture function $W(z)$ is formed in first area. This means that the optical wave must be rather wide. There is AO diffraction in the second area. The SAW aperture W_a (is about hundreds μm) defines the AO diffraction region dimension along the optical beam. This area is situated in a diffused optical waveguide on the lithium niobate crystal surface for the device. There are two optical waves in this area: the undiffracted wave and the diffracted wave. The diffracted wave has the information product of the optical and acoustical signals. The third area realizes two functions: separation diffraction optical beam (from input optical beam) and the AO diffraction image transmission to a CCD array. The separation is obtained on the property that undiffracted and diffracted beams have the different propagation angles.

Main purpose. To increase the efficiency of the methods we must use and a proposed make it possible to process both a synthesized optical aperture and a synthesized acoustic aperture.

The problems of theoretical researches, mathematical models, simulation and experimental investigation of the based on Y-cut lithium niobate crystal AO units for real time data processing are discussed.

The propagation of plane optical beams is analyzed in the diffraction approximation with a negligible diffraction distortion (they are quasi parallel) and Fraunhofer approximation [7] is reasonable in this case. So, it is possible to use Fourier transformation for longitudinal optical fields. We suppose that only the TE_0 - optical mode exists in a planar optical waveguide. For such a waveguide, we can split the Maxwell equations and consider the time and coordinate components. The analysis of the coordinate components yields a one dimensional mode equation and a two-dimensional wave equation (with effective refractive index N_{eff}). For the TE -mode polarisation of guide optical waves the mode Maxwell equation become according to equation [8]:

$$\frac{d^2 E}{d\rho^2} + (n^2(\rho) - N_{eff}^2)E = 0, \quad (1)$$

where $\rho = \kappa_0 y$, κ_0 is the optical wave number, E is optical field distribution normal to the boundary surface of the waveguide, $n(\rho)$ is function of refractive index profile (RIP) normal to the boundary surface of the waveguide. For titanium diffused waveguides the theoretical and experimental research leads us to a profile function for the refractive index given by [9]:

$$n^2(y) = n_s^2 + (n_0^2 - n_s^2) \left[(1 - \alpha) e^{-\left(\frac{y}{a}\right)^2} + \alpha e^{-\frac{y}{b}} \right], \quad (2)$$

where n_s is the substrate refractive index, n_0 - is the maximum the refractive index related to Ti-diffusion near the surface, a - is the effective depth of the Ti-profile, b - is the depth of the for out-diffusion, α - is the fraction of the exponential profile. This result was achieved by the optimization of the profile function comparing calculated and measured values of the effective refractive indices for multimode waveguides.

We study the propagation of light in the region of AO interaction assuming that the Bragg diffraction is realized, the properties of the waveguide mode remain unchanged, reflected waves are absent, the amplitude of the diffracted wave slowly increases (we can neglect the second derivation), and the perturbation of the waveguide permittivity caused by the SAW propagation is small [10,11]. The total diffraction losses are insignificant.

The diffraction efficiency of optical beam on SAW submits to the following parity [4,5]:

$$D = A^2(f) \left(\frac{\sin(qW_a)}{q} \right)^2, \quad \text{where } A^2(f) = \Gamma_{00}(f) P_{ac} - \text{AO interaction coefficient, } \Gamma_{00}(f) -$$

interaction integral for AO diffraction for TE_0 - TE_0 mode regime (the interaction integral for Y-cut lithium niobate crystal was learned in [11, 12], and it's the frequency dependent is shown on fig. 2a), f - SAW frequency, $P_{ac} = U_{eff}^2 Y_{IDT}$, U_{eff} - IDT supply voltage, Y_{IDT} - IDT

radiative transconductive, $q = \left(\frac{\Delta k}{2} \right)^2 + A^2$, Δk - disagreement wave vector (see fig. 2b), W_a - ITD aperture.

With allowance for the phase mismatch Δk [3], the relation between the amplitude functions of the incident and undiffracted $T_0(x)$ and diffracted $T_1(x)$ optical waves is determined by the solution to the equations of bound modes [10]. Using these assumptions, we can analytically solve the wave equations and derive integral expressions [5].

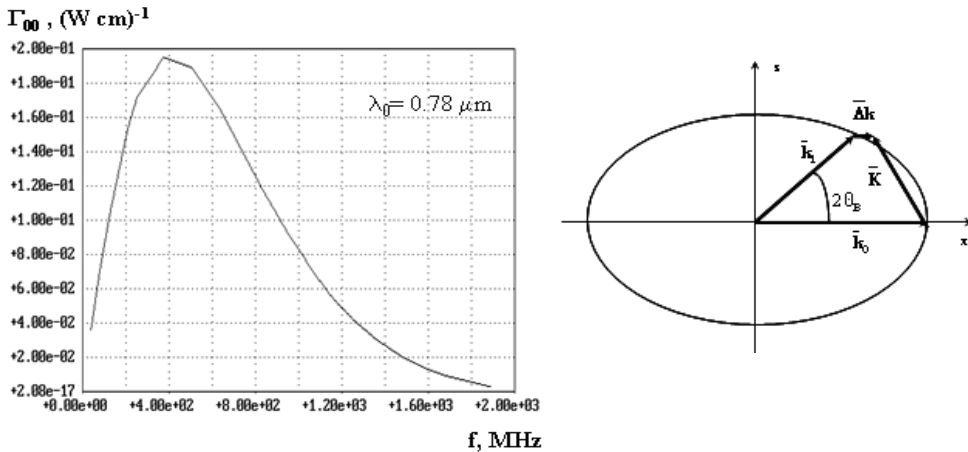


Fig. 2. (a) Plots of the frequency dependent of interaction integral for AO diffraction for TE₀-TE₀ mode regime, (b) The vector diagram of Bragg AO diffraction with disagreement optical wave vector

2. Real time multi-channel time-integrated correlation unit

2.1 Introduction

A classical time-integrated AO correlator (TIAOC) consists of a source of optical radiation (SOR), a collimating objective, an AO cell, an imaging objective, a spatial filter rejecting the null beam, and a CCD array [3, 13]. The main parameters of the AO correlator—the maximum delay time T_A . This parameter determines the range of delay times ΔT_A . The input signal $g_{in}(t)$ is used for time modulation of the light beam (for example, internal modulation of a laser or an LED). The second signal $h_{in}(t)$ modulates the amplitude of the acoustic wave with carrier frequency f_0 . This wave is used for space-time modulation of the transmittance of the acousto-optic cell. The Bragg diffraction angle of the optical beam corresponds to the carrier frequency of the acoustic wave. Since the incident light intensity and the cell transmittance are proportional to $g_{in}(t)$ and $h_{in}(t - z/V)$, respectively, the intensity distribution of the diffracted beam depends on the product $g_{in}(t)h_{in}(t - z/V)$. The cell image is projected on the CCD array, which integrates the intensity distribution with respect to time. The signal from the CCD array yields the spatial distribution of the correlation functions of signals $g_{in}(t)$ and $h_{in}(t)$.

2.2 Mathematical model of a mutli-channel WAOU for time-integrated correlation data processing in real time

One method for increasing the integration of the correlation channels is multicolor data processing [14]. In this case, a single device contains N independent correlators. The correlation channels employ optical beams with different wavelengths. This approach facilitates parallel data processing in real time, diminishes the operating costs of an individual acousto-optic correlation channel, and makes it possible to avoid crosstalk and intermode losses.

For the multi-channel TIAOC whose scheme is shown in fig. 3, the input signal $g_{in}(t)$ represents a superposition of N independent optical signals corresponding to different wavelengths λ_m , where $m = 1...N$. Each optical beam is amplitude modulated. The second input signal $h_{in}(t)$ represents a superposition of N independent electric signals, each of which generates a SAW at the corresponding frequency f_{om} and modulates its amplitude. The value of the carrier frequency is determined from the condition for the maximum in the overlap integral for the AO interaction of the SAW and the corresponding optical beam with a certain wavelength. Each optical beam is diffracted by the corresponding SAW in a waveguide AO Bragg cell (WBAOC). All cells are commoning the own chip. In the far-field region, the total diffracted optical field is a superposition of diffracted optical fields with different wavelengths. A prism is used in the focal plane of the imaging objective to spatially separate the optical beams. Thus, N independent correlation signals are simultaneously detected in the image plane in real time, which means that N independent correlation channels are realized in a single device.

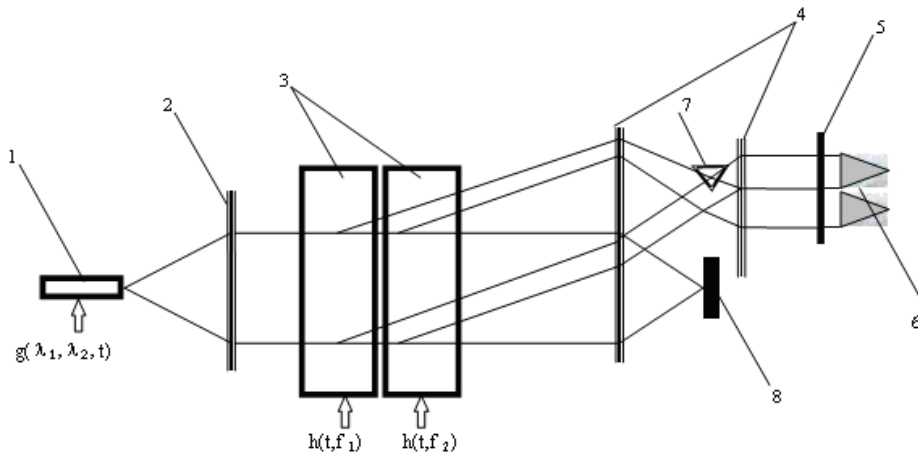


Fig. 3. Functional optical scheme of the multi-channel real time integrated TIAOC: 1 SOR, 2 collimating tens, 3 WBAOC, 4 image lens objective, 5 CCD array, 6 total correlation function 7 prism, 8 spatial filter. It's show two independent channel with deferent wavelengths).

Solid lines show typical paths of optical beams in the device from the SOR to the CCD-array.

With regard to the above conditions, the diffracted field of the m th optical wave obeys the following equation:

$$\Delta T_{1m}(x, z) + \left(\frac{2\pi}{\lambda_m} N_{effm}\right)^2 T_{1m}(x, z) = - \left[\int_{-\infty}^{\infty} dy k_{1m}^2 E_{0m}(y) E_{0m}^*(y) \right] T_{0m}(x, z) \tag{3}$$

where T_0 and T_1 are the longitudinal components of the incident and diffracted waves, respectively. Then, the distribution of the longitudinal component of the m -th diffracted optical wave is represented as

$$T_{1m}(x, z, t) = g_{inm}(t) \int_0^t d\tau R(z, t, \tau) h_{inm}(\tau),$$

$$R(z, t, \tau) = ie^{-i2\pi f_0 t} \int df e^{-i2\pi(f-f_0)(t-\tau)} A(\lambda_m, f_0_m + f)r(z) e^{i\frac{2\pi}{\lambda_m} N_{eff} (W a_m + \text{Sin} \frac{\Theta_m z}{2})}, \tag{4}$$

$$r(z) = \int d\eta W_{opt}(\eta) \int d\rho e^{-i2\pi\rho(z-\eta)} \text{Sinc} \frac{\Delta k_m(\rho) W a_m}{2} e^{i\frac{\Delta k_m(\rho) W a_m}{2}},$$

where f is the modulation frequency.

The optical field outside the waveguide is a 2D field, whose transverse size is mainly determined by the quantity W_{opt} and the diffraction broadening. In the first approximation, we can neglect the diffraction broadening of the beam, since its angular divergence is about 0.1×10^{-2} rad. The vertical size of the field depends on the ratio λ/n_{sub} . For the TE_0 mode, the field distribution along the vertical axis determined by (1) is close to the Gaussian distribution. Therefore, all effects are concentrated in the transverse cross section of the optical field. This makes it possible to analyze the propagation of light in the correlator under study in the one-dimensional approximation.

For known parameters of the imaging objective, the intensity distribution for the m th correlation channel in the image plane is given by

$$J_m(z) = \frac{1}{\sqrt{2} T_{int} R_{mag} \sigma} \int_0^{T_{int}} dt \int_{-\infty}^{\infty} d\xi I_{WBAOC_m} t_{in} t_{out} t_s e^{-\left(\frac{\xi + \Delta x - \frac{z}{R_{mag}}}{\sqrt{2}\sigma}\right)^2}, \tag{5}$$

where R_{mag} is the magnification of the imaging objective, T_{int} is time integrated, σ is the resolution of the imaging objective, and I_{WBAOC_m} is the integral intensity of the diffracted light for a m -th correlation channel, t_{in}, t_{out} are the translate coefficients of the prisms providing the chip incoupling/outcoupling of optical radiation, t_s is the translate coefficient of the prism providing the separation of optical radiation.

2.3 Computer simulation results

Using the model proposed, we theoretically analyze the values of the physical parameters of a hybrid five channel TIAOC. The WAOC consists of five WAOCs that serve as a time optical transparency. The lens system of the correlator is made up of volume objective lenses [15]. For the numerical calculations, we use the following parameters. The effective depths of the refractive index profile are 2.24 and 6.52 μm and $\Delta n^2 = 0.005$. The SAW velocity is 3488 m/s. Using these parameters, we perform computer simulation to optimize the IDT structure for each correlation channel. The value of the rectangular optical aperture function is $W_{opt} = 7$ mm. The resulting field is a superposition of independent optical fields corresponding to individual correlation channels. The spatial separation depends on the optical properties and configuration of the prism. The aperture and the focal length of the imaging objective are 120 and 16 mm, respectively. The magnification is $R_{mag} = 1/16$. Both input modulating signals are rectangular signals of equal duration. The computer simulation results predict complete separation of the diffracted and undiffracted optical beams in the focal plane of the imaging objective.

At the given values of the physical parameters, we numerically study the characteristics of a hybrid five channel TIAOC. The table 1 shows the main parameters of this device. Figure 4

demonstrates the results of the computer simulation of the diffraction patterns in the correlator image plane for various durations of the input signals. In the case under consideration, the total correlation function consists of five parts.

Parameters/correlation channel	1	2	3	4	5
1. Optical radiation wavelength in vacuum, μm	1,06	0,92	0,88	0,83	0,78
2. Maximum delay time T_A , μs	2	2	2	2	2
3. IDT parameters					
3.1. Central carrier frequency f_0 , MHz	251	277	321	380	436
3.2. Principal Bragg angle, deg.	1,0	1,1	1,2	1,3	1,5
3.3. Frequency bandwidth, MHz	14	15	16	16	18
3.4. Aperture, μm	380	400	400	420	450
3.5. Number of the fingers	53	51	49	47	41
3.5. Voltage standing-wave ratio in the working frequency range	1,2	1,2	1,2	1,2	1,2
4. Dynamic range, dB					
4. Dynamic range, dB	25	25	25	25	25
5. Minimum power of the RF signal, mW					
5. Minimum power of the RF signal, mW	90	70	60	50	50
6. Minimum power of the optical signal, mkW					
6. Minimum power of the optical signal, mkW	0,22	0,19	0,17	0,15	0,15

Table 1.

The maximum number of independent TIAOCs employing WAOCs based on the Y-cut lithium niobate substrate is 100.

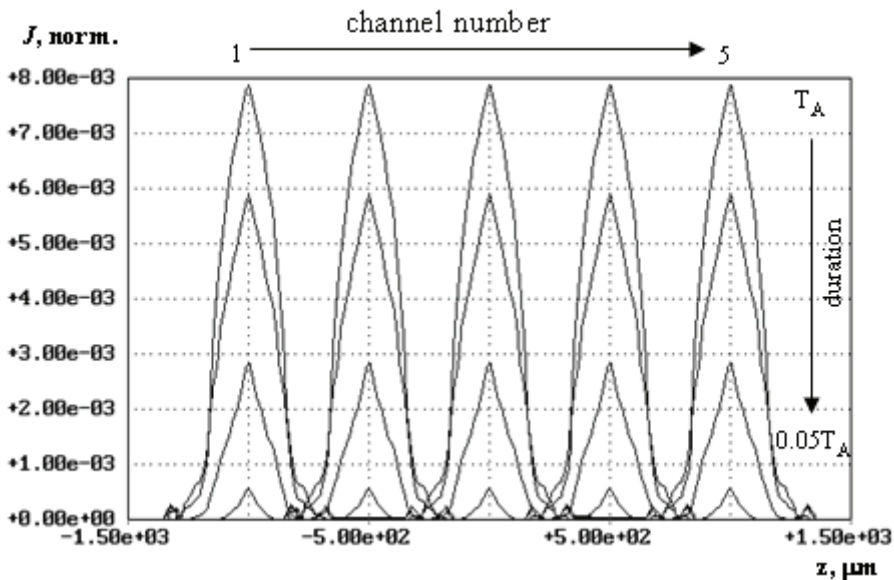


Fig. 4. Total correlation output signals for various durations of the input signals: from T_A to $0.05T_A$ (the delay time of $g_{in}(t)$ relative to $h_{in}(t)$ is $0.5T_A$). The families of curves correspond to the first (left-hand) to fives (right-hand) correlation channels, respectively

Using a mathematical model of the multi-channel TIAOC, one can also numerically analyze the characteristics of a hybrid monochrome TIAOC, in particular, at relatively small SAW variations. The validity of such an approach follows from the comparative analysis of the theoretical and experimental data. We employ an experimental prototype whose structure is described in detail in [16]. For the numerical calculations, we assume that, as in [16], WAOC contains a single WBAOC and two prisms providing the incoupling and outcoupling of optical radiation. The numerical experiments are performed for the wavelength in a vacuum $\lambda_0 = 0.78 \mu\text{m}$, the SAW velocity $V = 3488 \text{ m/s}$, and an optical aperture function whose value is 7 mm. The remaining initial data correspond to the experimental sample from [16]. Figure 5a demonstrates the results of the computer simulation and experimental data on the dependences of the normalized correlation peak height on the duration of the input signals at their relative duration of $0.5 T_A$. The experimental peak value is determined relative to the optical signal that is generated at the output of the device in the steady-state mode. The numerically calculated results can be presented in a similar way. Note also that the contributions related to additional biases applied to the optical source and WBAOC (pedestal contributions) are not taken into account in the results of the numerical calculations and experimental data.

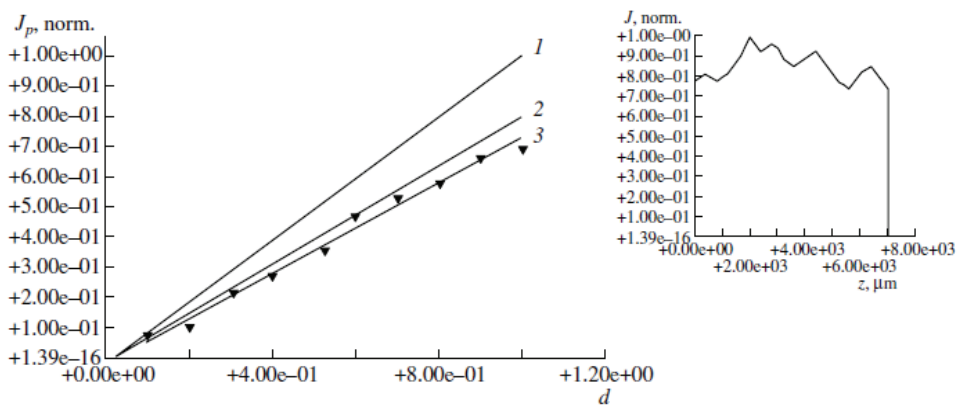


Fig. 5. (a) Plots of the normalized correlation peak height (J_p, norm) vs. duration (in fractions of T_A) of input signals at a relative delay of $0.5T_A$: (1) rectangular optical aperture function, (2) experimental optical aperture function, (3) experimental data from [16], and (triangles) experimental points. (b) Experimental optical aperture function.

Based on the comparative analysis of the numerical and experimental data, we draw the following conclusion. The proposed mathematical model can be used to analyze the affect of variations in the SAW velocity on the correlation signal, since both dependences are linear. However, the slope of the calculated curve differs from the slope of the experimental curve. This is due to the fact that the shape of the experimental aperture function significantly differs from the rectangular shape. The real shape is important in the calculation of the parameters of the given TIAOC. For comparison, Fig. 5a shows similar results calculated with allowance for the shape of the aperture function used in the experiments (Fig. 5b). In this case, the slopes are virtually identical.

2.4 Conclusion

We propose an AO method for time-integrated multi-channel correlation data processing in real time. This method enables one to significantly increase the number of independent correlation channels. We develop a mathematical model of a multicolor AO device for real-time correlation analysis with time integration. We theoretically and numerically analyze the characteristics of a hybrid five channel correlator, whose AO chip is based on the Y-cut lithium niobate substrate. Multi-channel AO correlators with time integration make it possible to simultaneously detect up to 100 correlation functions provided that Y-cut lithium niobate serves as the substrate.

3. Bandwidth AO unit for the real-time spectrum analysis of optical signals

3.1 Introduction

The design and development original AO method for the real-time spectral analysis of broadband optical signals are discussed. The unit implemented this mean allows for the real-time processing of an optical signal that exhibits a complicated spectrum with hundreds of components. This unit may also serve as a high-accuracy real-time optical-frequency detector working in a wide spectral range.

Figure 6 shows that the classical AO unit consists of three components: optical port (1), waveguide AO chip (2), and photodetector unit (3). The optical signal from the first unit is fed to the WAOC, where it is collimated with an aplanatic lens (4) to a wide-aperture plane wave (5). Then, the wave propagates through the region of the perturbed planar waveguide (6), which is induced by the propagating surface acoustic wave (7) generated by an electroacoustic IDT (8). In this case, the Rayleigh SAW with strictly fixed frequency f_0 serves as an optical transparency. Then, a component of the optical signal is deflected due to Bragg diffraction by the angle [10]

$$\Theta_m = \frac{\lambda_m}{V} f_0, \quad (6)$$

where λ_m is the radiation wavelength of the m-th component in the waveguide.

The number of the diffracted optical beams corresponds to the number of the frequency components of the original optical signal. The resulting diffraction field is focused with an aplanatic lens (9) on the end of the waveguide and is detected with a photodetector array (3).

The mathematical model of the waveguide AO spectrum analyzer of the optical radiation is similar to the well-developed and experimentally tested model of the waveguide AO spectrum analyzer of radio signals [16]. The differences are as follows: first, the parameter under study is the radiation wavelength rather than the radio frequency (which is fixed); second, the chromatic dependence of the overlap integral of the Bragg AO interaction needs to be taken into account.

The optical wave diffracts on SAW. Thus the diffraction efficiency of an each optical component submits to the following parity:

$$D = A^2(\lambda_m, f_0) \left(\frac{\sin(q_m V_a)}{q_m} \right)^2, \quad (7)$$

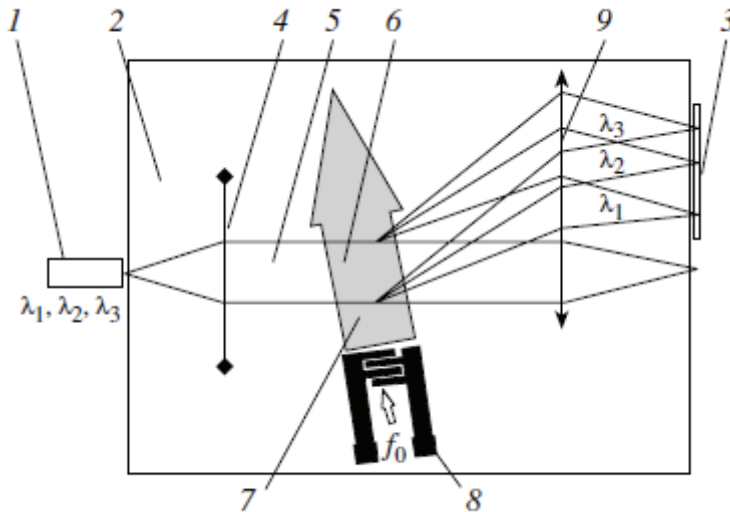


Fig. 6. Scheme of the waveguide Bragg AO device for the real-time spectral analysis of the broadband optical signals: solid lines show optical beams.

where $A^2(\lambda_m, f_0) = \Gamma_{00}(\lambda_m)P_{ac}$ - AO interaction coefficient for m-th optical component, $\Gamma_{00}(\lambda_m)$ - chromatic interaction integral for AO diffraction for TE_0 - TE_0 mode regime,

$q_m = \left(\frac{\Delta k_m}{2}\right)^2 + A^2(\lambda_m, f_0)$, Δk_m - disagreement wave vector for corresponding optical component.

The frequency of a everyone diffracted optical beam will be moved on frequency f_0 . And the quantity of diffracted optical beams corresponds to quantity of frequency components of an initial signal.

In general, the band of the working optical frequencies is bounded by the SAW excitation band, the AO interaction band, the frequency band of the overlap integral, which characterizes the AO properties of the material, and the band of the optical frequencies in which the planar waveguide supports a single TE_0 mode. The last two parameters are significantly more important than the first two parameters. A single IDT is insufficient for the analysis of the broadband optical signals, since the band of the analyzed optical frequencies is relatively narrow (about 100 nm) [4, 5]. In contrast to the monochromatic case, the characteristic is strongly asymmetric, since the overlap integral decreases with increasing wavelength at relatively large $\Delta\lambda$. For this reason, a multiple-IDT system is used to increase the width of the frequency band. In this system, the crossed structure of acoustic beams enables one to maximize the diffraction efficiency. Several IDTs that excite SAW are placed at the Bragg angle relative to the propagation direction of the channeled radiation. The complexity of this scheme lies in the manifestation of the interference effects for the optical beams diffracted by different SAW beams. This leads to a significant nonuniformity of the frequency characteristic. To solve this problem, we need to employ computer simulation for the amplitude and phase tuning of the device (both the topological parameters of the cell and the electric circuit for the matching of the IDT and RF systems are tuned). It is demonstrated in [5] that the amplitude and phase matching is stable only for three IDT's.

3.2 Mathematical model of AO units for the real-time spectrum analysis of bandwidth optical signals

In case greatest possible value (~300 nm) of a bandwidth of an optical signal (such signals can propagated in waveguide at only TE_0 -mode regime) use 3 ITD obviously insufficiently. One of ways of increase of a optical frequency bandwidth is entering an additional mismatch of wave vectors with the purpose of increase of a total optical frequency bandwidth, but as the consequence is observed decrease of diffraction efficiency. This approach is realised by change of value of a angle between an optical beam and SAW front, that is achieved additional turn of the ITD. Thus should be satisfied condition:

$$\frac{\sin(q_i W_{a_i})}{q_i} = \left[\frac{\pi}{2} (4n + 1) \right]^{1/2}, \tag{8}$$

where $n=0,1,2,3$.

Thus the diffraction efficiency of a each optical component submits to a parity (7). The regime of low diffraction efficiency allows to simplify parities describing optical fields:

$$\begin{aligned} T_0 &= const \\ T_1 &= -i \frac{A(\lambda_m) T_0}{\Delta k} e^{-i(\Delta k x + \Phi(z))}, \end{aligned} \tag{9}$$

where T_0 - longitudinal initial optical field component, T_1 - longitudinal diffracted optical field component, $\Phi(z)$ - phase of longitudinal diffracted optical field component [4,5].

The optical field each wave components is the sum an optical field generated appropriate SAW, extending under different angles to an initial optical beam. Presence several coherent the optical field results in them interference. Then the optical field separate wave components under condition of low efficiency diffraction submits to the following parity:

$$T_{1_m}(x) = -i \frac{A(\lambda_m) T(x) e^{-i(\Delta k_1 x + \Phi_1(z))}}{\Delta k_1} \left(1 + \sum_{j=2}^N \frac{\Delta k_1}{\Delta k_j} e^{-i((\Delta k_j - \Delta k_1)x + (\Phi_j(z) - \Phi_1(z) + \Phi_{opt}))} \right). \tag{10}$$

The given field by means of an integrating lens is transferred on a ruler of photoreceivers placed in a lens focal plane. The intensity distribution of each wave component in a focal plane of an integrating lens is described by parity [17]:

$$\begin{aligned} W_{F_m}(x_0, z) &= \int_{-\infty}^{\infty} d\xi \frac{(1 + \phi)}{\sqrt{s}} T_{1_m}(\xi, \eta) e^{-i(\Phi_2(z) + k_o N_{eff}(\psi) s \cos(\psi))}, \\ s &= \sqrt{(x_0 - \eta)^2 + (z - \xi)^2} \end{aligned} \tag{11}$$

where s - the distance from the point on last lens contour to the observation point, ϕ - the angle between the ray coming to the point ξ to point (x_0, z) , ψ - the angle between the phase and group velocity for the ray directed towards the observation point, $\Phi_2(z)$ - the phase of optical ray at the point ξ .

The total optical field is superposition of fields a each optical component.

An increase in the aperture function leads to an additional decrease in the sensitivity of the frequency characteristic to the interference effects. This is due to the averaging of the phases

of the diffracted beams. It follows from the analysis of the phase dependences of the interfering beams that the interference effects are completely eliminated provided that the optical aperture satisfies the following condition:

$$W_{\text{opt}} \gg \frac{\Delta\lambda}{4\Delta\Theta^2} \quad (12)$$

where $\Delta\lambda$ is the wavelength band of the analyzed radiation and $\Delta\Theta$ is the difference between the Bragg angles of the neighboring IDT's. For the typical parameters $\Delta\lambda = 100$ nm and $\Delta\Theta = 0.0017$, condition (12) is satisfied for an optical aperture of about 100 mm. However, such large apertures cannot be technically realized in the integrated optical devices, and the aforementioned property provides for only partial compensation of the interference effects.

3.3 Computer simulation results

We develop two modifications of the AO devices for the spectral analysis of the red and IR broadband optical signals. In these devices are based on Y-cut lithium niobate. The refractive index profile of diffusion planar optical waveguide is described the following parameters. For the first modification, the effective depths are 2.24 and 6.52 mkm and $\Delta n^2 = 0.005$. For the second modification, the effective depths are 2.42 and 6.12 mkm and $\Delta n^2 = 0.008$. TIPE technology [18] is used to fabricate aplanatic lenses. We assume that the optical aperture function is nearly Gaussian and its values for the first and second modifications are $W_{\text{opt}} = 5$ and 7 mm, respectively. The SAW velocity is 3488 m/s. Based on these parameters, we employ computer simulation to optimize (i) the IDT-system design with respect to the maximization of the band of the analyzed optical frequencies and (ii) the topology of the lens system with respect to the maximization of the optical resolution using the method proposed in [19]. The table 2 demonstrates the main parameters of the two modifications obtained with the numerical and experimental study.

Parameters	Mod. 1		Mod. 2
	simul.	exper. [16]	simul.
1 Optical radiation waveguide range			
- low wavelength, nm,	600	605	765
- high wavelength, nm,	935	915	1125
2 Working wavelength band, nm	335	315	360
3 Resolution of two optical wavelengths, nm,	2.9	3.5	3.1
4 Measuring fixed frequency for RF signal, MHz	394	396	326
5 Diffraction efficiency, %/W	1.5	0.8	0.3
6 Dynamic range, dB	25	23	25
7 Low level of measured optical signal, μW	10	10	10
8 Input RF signal power level, W	0.4	0.6	1.2
9 Voltage standing wave ratio for driving RF signal	1,8	2	1.8

Table 2.

Figure 7a shows the numerically calculated dependence of the optical transmittance of the first modification on the wavelength. At a level of -3 dB, the working wavelength band is slightly greater than 335 nm in the range from 935 to 600 nm. For comparison, we also present the experimental characteristic of this AO device from [16]. Figure 7b shows the wavelength dependence of the calculated optical transmittance for the second modification. At a level of -3 dB, the working wavelength band is 360 nm in the range from 1125 to 765 nm. Note that the parameters of the device are chosen with allowance for the technological requirements for its fabrication. A working band of 360 nm is the ultimate band for the single mode diffusion waveguides under study [14]. The optical signals with such maximum bandwidth can be supported with the waveguides under study in the IR range

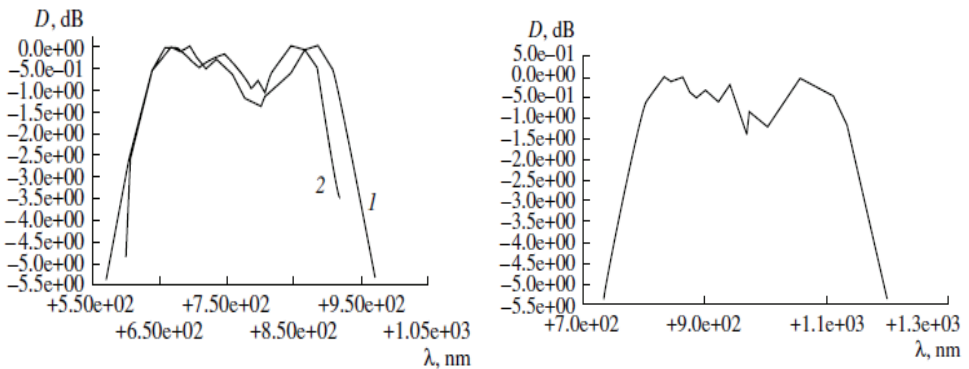


Fig. 7. Plots of optical transmittance D vs. wavelength for (a) the first modification of the spectrum analyzer, (b) for the second modification of the spectrum analyzer.

The comparative analysis yields a good agreement between the theoretical and experimental data on the first modification. In particular, the difference between the RF signals is less than 1%, the difference between the central optical frequencies is almost 10%, and the difference between the working transmission bands is less than 10%.

Figure 8 demonstrates the experimentally determined accuracy of the measurement of the optical signal wavelength with the first modification in which a laser diode serves as the source of the optical signal.

The left panel shows the typical response of the device. At a fixed frequency of the RF signal and a stable radiation of the laser diode, the response is symmetric (Fig. 8a). A variation in the input current of the laser diode leads to a variation in the radiation wavelength, which causes a variation in the response (Fig. 8b). In this case, the voltage difference between the N th and $(N + 1)$ th pixels is 0.2 V. The response can be symmetrized by tuning the oscillator frequency. The difference between the oscillator frequencies is 38 kHz. Thus, the wavelength of the laser diode is varied by 0.054 nm. In practice, we can observe and measure a voltage difference of about 10 mV between the $(N - 1)$ th and $(N + 1)$ th pixels. Hence, the ultimate accuracy of the wavelength measurement for the optical signal in the device under study is no worse than 0.01 nm.

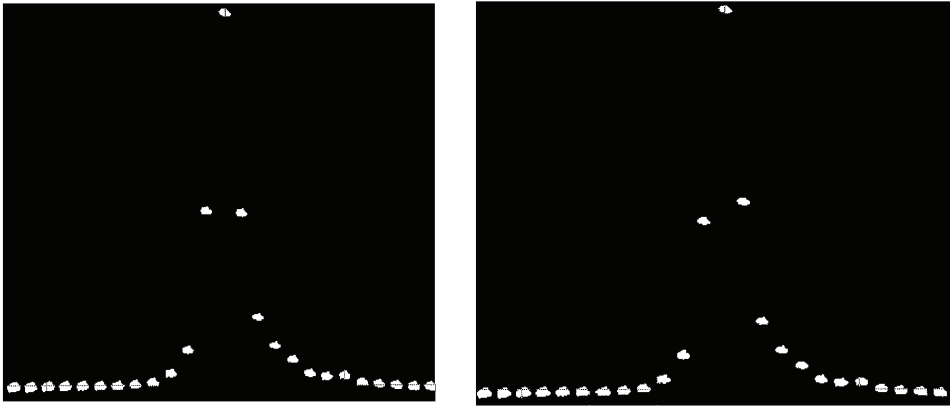


Fig. 8. Photographs of the responses for the first modification of the AO device.

3.4 Conclusion

We developed and numerically studied two modifications of the AO device for the spectral analysis of broadband red and IR optical signals. We employ a mathematical model which is similar to the experimentally tested mathematical model of the waveguide AO analyzer of radio signals. The comparative analysis yields a good agreement between the theoretical and experimental results. The band of the working optical frequencies is 360 nm in the range 765–1125 nm. The wavelength resolution of the two optical signals determined with the Rayleigh criterion is 3 nm. The optical wavelength is measured with an accuracy of 0.01 nm. The minimum level of the analyzed optical signal is 10 mW. In particular, the differences between the RF signals, the central optical frequencies, and the working transmission bands are less than 1%, almost 10%, and less than 10%, respectively. The parameters of the device are chosen based on the real technological and topological requirements for its elements.

4. Methods for real-time optical scanning of large data arrays

4.1 Introduction

A distinctive feature of the methods proposed is a significant increase in the number of scanning points (information bits) in comparison to the classical method involving spectral analysis of broadband RF signals based on waveguide AO Bragg interaction [4, 16]. In a conventional scanning system, the frequency of the controlling RF signal fed to a scanning unit is discretely varied within the frequency band of the device. A variation in frequency leads to a variation in the diffraction angle of the optical beam [10]:

$$\Theta_{dif} = \Theta_o + \arcsin\left(\frac{\lambda_o f}{N_{eff} V} - \sin \Theta_a\right) \quad (13)$$

where Θ_o is the angle between the fronts of the optical beam and surface acoustic wave, and Θ_a is the angle between the SAW propagation direction and the z axis.

A variation in the diffraction angle causes a shift of the focused optical beam to the neighboring point in the focal plane coinciding with the side surface of the waveguide. The

scanning is thus realized. The discrete step in the frequency variation depends on the frequency resolution of the optical focusing system [4]. The number of scanning points is given by

$$N_T = \frac{\Delta f}{R_f} \tag{14}$$

where Δf is the frequency band and R_f is the resolution of the focusing optical system.

The hardware for realizing the above method employs a source of optical radiation and a waveguide acoustooptic chip. The chip contains a planar optical waveguide, optical input/output elements, an optical system consisting of collimating and focusing lenses, and a waveguide AO Bragg cell. Note that for scanner elements based on Y-cut lithium niobate, the number of scanning points is no greater than 1000 for the ultimate values of Δf and R_f [4]. However, the technical realization of such a device is difficult and expensive [16].

4.2 Method for one-dimensional scanning

A conventional method for 1D scanning can be improved to achieve a significant increase in the amount of data processed in real time using an approach that employs a synthesized (with a few optical beams) aperture of the optical field. The total information field is divided into subareas, each of which is irradiated with an individual optical beam controlled by the corresponding WAOBC. In the case under consideration, the first optical beam is incident on the corresponding cell at an angle Θ_{max} equal to a double Bragg angle corresponding to the upper bound limit of the cell working frequency range. The next optical beam is incident on the second WAOBC at an angle $\Theta_{max} + \Delta\Theta_c$, where $\Delta\Theta_c$ is the working range of angles of the previous cell. In the general case, the angle of incidence of the current optical beam differs from the previous one by $\Delta\Theta_c$ (Fig. 9). Thus, the scanning range increases by a factor of M , where M is the number of cells.

A similar WAOBC system is placed symmetrically with respect to the optical axis. Note the matching of the working range of angles of the focusing system (Θ_L) and the total working range of the WAOBC system. Hence, the number M satisfies the following condition:

$$M < \frac{\Theta_L}{2\Delta\Theta_c} \tag{15}$$

Thus, the total number of scanning points is given by

$$N_{T_{total}} = 2MN_T \tag{16}$$

We investigate the propagation of a monochromatic coherent quasi-plane optical wave with a predetermined aperture function $W(z)$. We assume that the AO Bragg phase matching condition [5] is satisfied, the diffraction efficiency is about a few percent. In the general case, the aperture of the surface acoustic field is synthesized with a few electroacoustic IDTs. In the far-field zone, the electrical component of optical field diffracted by a each WAOBC is represented as

$$T_1(x, z, t) = T_0(x) \int_{-\infty}^{\infty} dk_z \sum_{j=1}^N \frac{A_B(f)}{\Delta k(x, z)} (e^{i\Delta k W_{aj}} - 1) e^{-i((\omega \pm \Omega)(t - T_a) - N_{eff}(\sqrt{k_0^2 - k_z^2})x + \Phi_B(x, z, f) + Kz)} e^{-\alpha(f)z} \tag{17}$$

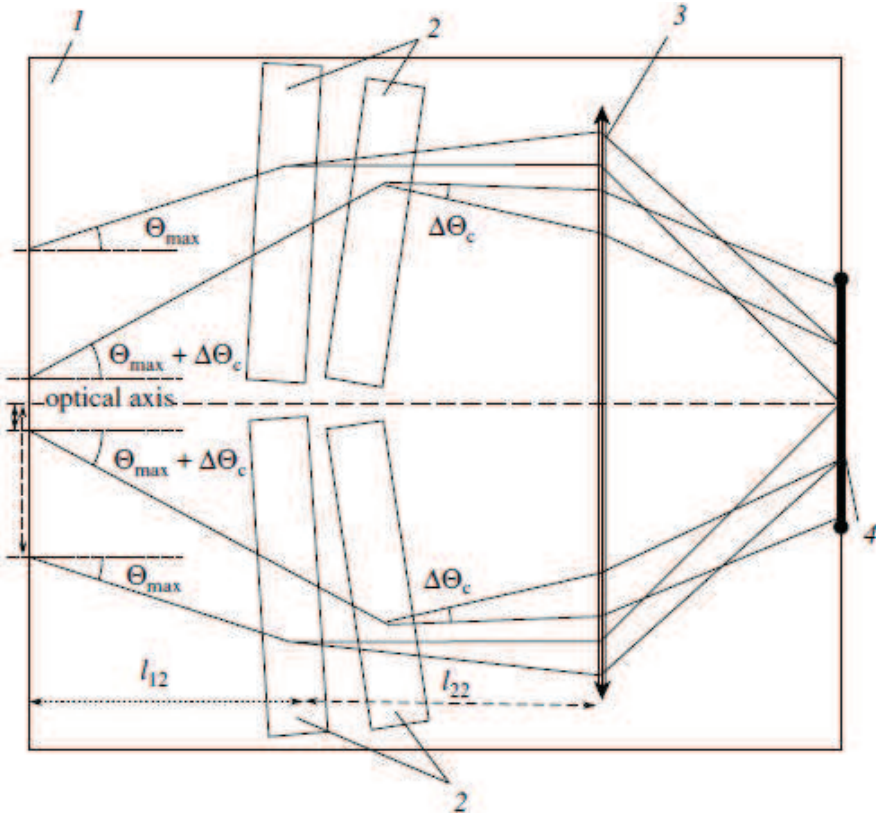


Fig. 9. Functional scheme of the waveguide AO scanning device: 1 WAOC, 2 WAOBC, 3 focusing lens objective, and 4 total information field. Solid lines show typical paths of optical beams in the device from the SOR to the scanning region. The SOR and collimating lens system are not shown.

where ω and k_0 are the frequency and wave number of the TE_0 mode; Ω and K are the frequency and wave number of the SAW; $A_B(f)$ is the Bragg AO interaction coefficient corresponding to parameter $A(f)$, determined in sec. 1., N is the number of IDTs; W_a is the j -th IDT aperture; $\Phi_B(x, z, f)$ is the phase related to the RF electric signal passing through the matching electric circuit, SAW propagation from the electroacoustic transducer to the region of acoustooptic interaction, and interference depending on the acoustic field topology [5, 11]; and $\alpha(f)$ is the SAW decay coefficient, which was analyzed in detail in [6]. This field is focused using a waveguide lens objective with focal length F . In the back focal plane of the objective, the field distribution is represented as

$$W_F(x_F, z) = \int_0^{T_{Sc}} d\tau \int_{-\infty}^{\infty} d\xi \frac{(1 + \phi)}{\sqrt{s}} T_1(\xi, \eta, \tau) e^{-i(\Phi_2(s) + k_0 N_{eff}(\psi) s \cos(\psi))} \tag{18}$$

where T_{Sc} is the scanning time.

4.3 Computer simulation results

Using the above approach, we developed a AO planar scanning device based on Y-cut lithium niobate. This device makes it possible to selectively process more than 3000 information bits in real time. The device consists of four WAOBCs (two cells on each side of the optical axis). It is possible to arbitrarily control the cells. Using the model proposed, we numerically study the characteristics of this scanner working in real time. In numerical experiments, we employ the following typical initial data presented in the table 3. The aperture function of the optical beam is nearly Gaussian, and the corresponding value is $W_{opt} = 5$ mm.

Parameter	
Planar waveguide	
Effective refractive index for TE ₀ mode	2.19176
Difference between maximum refractive indices of the waveguide and substrate	0.8×10^{-2}
Depth of the Gaussian profile, μm	2.42
WAOBC parameters	
Total working frequency range at a level of 3 dB, MHz	1090
Range of diffraction angles, rad	0.111
Maximum diffraction efficiency, %/W	0.97
Number of sections in the first IDT	17
Aperture of the first IDT, μm	450
Number of sections in the second IDT	23
Aperture of the second IDT, μm	280
Electric power of the RF signal, W	0.6
Voltage standing-wave ratio in the working frequency range	less than 2
Parameters of the optical lens system	
Difference between maximum refractive indices of the TIPE lens and substrate	
Effective depth of the TIPE lens, μm	0,0328
Focal length of the collimating system, mm	4.24
Number of lenses of the focusing objective	2
Focal length of the focusing objective, mm	35
Aperture of the focusing objective, mm	15.8
Size of the scanning optical spot, mkm	0.22
Main characteristics of the WAOBC	
Number of WAOBCs	4
Aperture of the optical beam, mm	5
Angle between the optical axis and the optical beam for the first WAOBC, rad	0.130
Angle between the optical axis and the optical beam for the second WAOBC, rad	0.240
Total number of scanning points	4360

Table 3.

Thank You for previewing this eBook

You can read the full version of this eBook in different formats:

- HTML (Free /Available to everyone)
- PDF / TXT (Available to V.I.P. members. Free Standard members can access up to 5 PDF/TXT eBooks per month each month)
- Epub & Mobipocket (Exclusive to V.I.P. members)

To download this full book, simply select the format you desire below

